ACS APPLIED MATERIALS & INTERFACES

Research Article

www.acsami.org

Highly Dispersible and Stable Copper Terephthalate Metal–Organic Framework–Graphene Oxide Nanocomposite for an Electrochemical Sensing Application

Xia Wang, Qingxiang Wang,* Qinghua Wang, Feng Gao, Fei Gao, Yizhen Yang, and Hongxu Guo

College of Chemistry and Environment, Fujian Province Key Laboratory of Morden Analytical Science and Separation Technology, Minnan Normal University, Zhangzhou, Fujian 363000, P. R. China

ABSTRACT: A highly dispersible and stable nanocomposite of Cu(tpa)-GO (Cu(tpa) = copper terephthalate metal–organic framework, GO = graphene oxide) was prepared through a simple ultrasonication method. The morphology and structure of the obtained composite were characterized via scanning electron microscopy (SEM), transmission electron microscopy (TEM), UV–vis, Fourier-transform infrared (FT-IR), X-ray diffraction (XRD), and thermogravimetric analysis (TGA). On the basis of the characterization results, the binding mechanism of the Cu(tpa) and GO was speculated to be the cooperative interaction of $\pi-\pi$ stacking, hydrogen bonding, and Cu–O coordination. The electrochemical sensing property of Cu(tpa)-GO composite was investigated through casting the composite on a glassy carbon electrode (GCE), followed by an electro-reduction treatment to transfer the GO in the composite to the highly conductive reduced form (electrochemically reduced graphene, EGR). The results demonstrated that the electrochemical signals and peak profiles of the two drugs of acetaminophen (ACOP) and dopamine (DA) were significantly improved by the modified material, owing to the synergistic effect from high conductivity of EGR and unique electron mediating action of Cu(tpa). Under the optimum conditions, the oxidation peak currents of ACOP and DA were linearly correlated to their concentrations in the ranges of 1–100 and 1–50 μM, respectively. The detection limits for ACOP and DA were estimated to be as low as 0.36 and 0.21 μM, respectively.

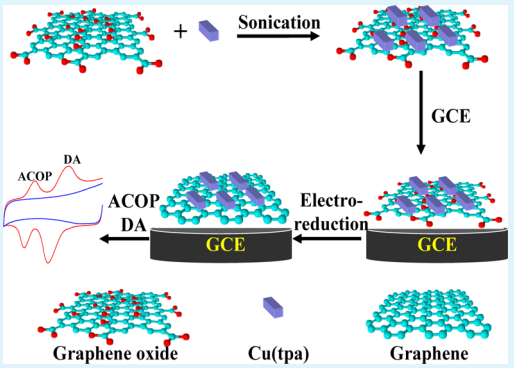

KEYWORDS: *graphene oxide, copper terephthalate metal–organic framework, acetaminophen, dopamine*

1. INTRODUCTION

Nanoscale porous materials have received enormous attention in the past decade, because of their potential application in gas adsorption,[1] catalyst supports for electric double layer capacitors,[2,3] and fuel cells.[4] Among the various porous materials, metal–organic frameworks (MOFs), also known as coordination polymers or coordination networks, have attracted much interest because of their high accessible surface areas, tunable pore sizes, open metal sites, and ordered crystalline structures.[5,6] MOFs are also of fundamental interest and practical use in electrochemistry, because many metal ions used in MOFs are electrochemically active.[7] Therefore, in the recent years, the application of MOFs in the electrochemical field receives growing concerns.[8,9]

However, the direct application of single component MOFs in electrochemistry is limited due to their poor electronic conductivities, low mechanical stabilities, and inferior electrocatalytic abilities.[10,11] In order to overcome these disadvantages, the introduction of the other highly conductive and mechanically durable materials into MOFs has been proposed. For example, Zhang et al.[10] have reported a Cu-based MOF/macroporous carbon (MPC) hybrid material. The electrochemical experiments showed that the incorporation of MPC greatly enhanced the stability and electrocatalysis of the Cu-based MOF. In addition, Hosseini et al.[11] prepared an Au-SH-SiO_2 nanoparticles/Cu-MOF composite modified electrode and used it as a highly sensitive and selective sensor for the electrochemical determination of L-cysteine. Nevertheless, these materials suffer from the drawbacks of a complicated synthesis process and low dispersibility and stability in the water solution, which greatly inhibits their wider practical application in the electrochemical field.

In this work, a novel hybrid nanocomposite of copper terephthalate MOF-graphene oxide (Cu(tpa)-GO) with excellent dispersibility and stability in aqueous solution was synthesized through a simple and effective sonication method. The morphology and structure of the obtained composite were characterized using scanning electron microscopy (SEM), transmission electron microscopy (TEM), UV–vis, Fourier-transform infrared (FT-IR), X-ray diffraction (XRD), and thermogravimetric analysis (TGA). The binding mechanism of the Cu(tpa) and GO was speculated to be the cooperative interaction of $\pi-\pi$ stacking, hydrogen bonding, and Cu–O coordination. Then, the Cu(tpa)-GO nanocomposite was cast

Received: April 16, 2014
Accepted: July 7, 2014
Published: July 7, 2014

on a glassy carbon electrode (GCE) and treated electrochemically to transform the GO to the reduced form, namely, electrochemically reduced graphene (EGR), possessing the higher accessible surface area and conductivity.[12−14] To explore the potential of the Cu(tpa)-EGR hybrid, the modified electrode was used as an electrochemical sensing platform for the determination of acetaminophen (ACOP) and dopamine (DA). The results showed that the two drugs exhibited well separated and enhanced redox peaks on the modified electrode, which opens a new avenue to extend the potential electrochemical application of the MOFs materials. Therefore, this study provided a theoretical and practical basis to prepare highly dispersible and stable MOF-based composites and demonstrated their promising applications in the electrochemical field.

2. EXPERIMENTAL SECTION

2.1. Chemicals. ACOP and terephthalic acid (TPA) were obtained from Sinopharm Chemical Reagent Co., Ltd. (P. R. China). DA and copper nitrate trihydrate ($Cu(NO_3)_2{\cdot}3H_2O$) were purchased from Aladdin Reagent Co., Ltd. (P. R. China). Graphite powder was obtained from Guangdong Xilong Chemical Co., Ltd. (P. R. China). Phosphate-buffered saline (PBS) with different pH values was prepared by mixing 0.02 M NaCl and 0.5 M NaH_2PO_4–Na_2HPO_4. All the other chemicals were of analytical grade and used without further purification. Doubly distilled water (DDW) was used throughout the experiments, and all assays were performed at room temperature.

2.2. Apparatus. Scanning electron microscopy (SEM) was performed using a Hitachi model S-4800 microscope (Japan). X-ray diffraction (XRD) was operated on a Bruker D8-Advance X-ray diffractometer (Germany). Fourier-transform infrared (FT-IR) spectra were recorded using a Bruker Tensor 27 spectrometer (Germany). UV−vis absorption spectra were obtained with a Shimadzu UV-2550 spectrophotometer (Japan). Thermogravimetric analyses were conducted on a TGA Q600 thermal degradation analyzer (USA) with a heating rate of 10 °C under N_2. Electrochemical experiments were measured on a CHI 650D electrochemical workstation (P. R. China) with the conventional three-electrode system consisting of a bare or modified GCE (Φ = 3 mm) as working electrode, platinum wire as counter electrode, and Ag/AgCl (saturated KCl solution) as reference electrode. All potentials were measured and reported versus Ag/AgCl. The pH values were measured on a model pHS-25 digital acidometer (P. R. China).

2.3. Preparation of Cu(tpa)-GO Nanocomposite. GO was synthesized from natural graphite powder by a modified Hummers' method.[15] The Cu(tpa) MOF was synthesized by a modified published procedure.[16,17] In brief, 40 mL of DDW with 5 g of $Cu(NO_3)_2{\cdot}3H_2O$ was mixed with 2 g of TPA dissolved in the mixing solvent of 40 mL of *N*,*N*-dimethylformamide (DMF) and 40 mL of ethanol. Then, the mixture was treated with a solvothermal method at 85 °C for 24 h. The blue powder was recovered by filtration, washed with water and DMF, and dried at 80 °C under vacuum. The Cu(tpa)-GO nanocomposite was prepared by adding 1 mg of Cu(tpa) to 1 mg mL^{-1} aqueous GO under stirring, followed by sonication at 100 W for 1 h to obtain a homogeneous dispersion.

2.4. Fabrication of the Cu(tpa)-EGR Modified GCE. Prior to modification, the bare GCE was polished to a mirror-like surface sequentially with 1.0, 0.3, and 0.05 μm α-Al_2O_3 and then rinsed ultrasonically with DDW, ethanol, and DDW. The cleaned electrode was dried under a high-purity N_2 stream. Then, 10 μL of Cu(tpa)-GO suspension was cast onto the electrode surface. After dryness under room temperature, the modified electrode was carefully rinsed with DDW to remove loosely attached Cu(tpa)-GO; thus, the Cu(tpa)-GO modified GCE (Cu(tpa)-GO/GCE) was obtained. For comparison, the Cu(tpa) modified GCE (Cu(tpa)/GCE) and GO modified GCE (GO/GCE) were prepared only by replacing the Cu(tpa)-GO dispersion with Cu(tpa) or GO solutions.

The reduction of GO in the Cu(tpa)-GO film was performed electrochemically as described in the literature.[18] Briefly, Cu(tpa)-GO/GCE was immersed in 0.1 M PBS (pH 7.0) and circularly scanned between −1.5 and 0.6 V until steady curves were achieved. The obtained electrode was denoted as Cu(tpa)-EGR/GCE. The EGR modified electrode (EGR/GCE) was prepared by the similar electrochemical reduction of GO/GCE in 0.1 M PBS (pH 7.0).

2.5. Electrochemical Measurements. Electrochemical characterizations of the modified electrodes were performed in 0.1 M PBS (pH 7.0) through a cyclic scan in the potential range from −1.0 to 0.8 V. The electrochemical sensing test of the modified electrode was carried out in the following procedure: Appropriate amounts of ACOP and DA standard solution were added into 0.1 M PBS (pH 5.0), and then, cyclic voltammetric (CV) and differential pulse voltammetric (DPV) measurements were recorded. CVs were recorded in the potential range from 0 to 0.80 V. DPVs were recorded at an increment potential of 0.004 V, pulse amplitude of 0.05 V, pulse width of 0.05 s, sample width of 0.0167 s, pulse period of 0.2 s, and quiet time of 2 s. Scheme 1 shows the preparation of Cu(tpa)-EGR/GCE and its application for sensing analysis of ACOP and DA.

Scheme 1. Illustration for the Sonication-Assisted Preparation of Cu(tpa)-GO and Its Application for the Simultaneous Determination of ACOP and DA

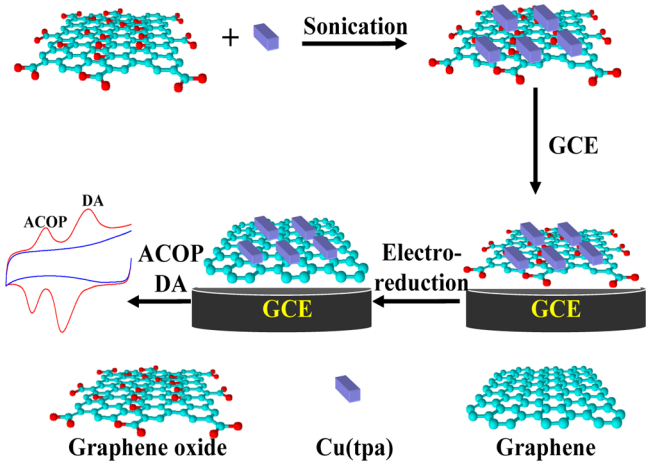

3. RESULTS AND DISCUSSION

3.1. Materials Characterization. Figure 1A displayed the SEM image of the synthesized Cu(tpa) particles, in which a large amount of regular and independent cuboids were observed, indicating high yield and good crystallinity of the Cu(tpa) MOF. From the higher magnification image (inset of Figure 1A), it could be seen that the large cuboids generally consisted of two to four small cuboids with a diameter of about 100 nm. The SEM image of the sonication-prepared Cu(tpa)-GO composite showed that the Cu(tpa) particles in the composite remained in their original cuboid shape (Figure 1B), indicating that the sonication treatment used in the preparation of the composite had no effect on the morphology of the Cu(tpa) MOF. Moreover, from the local amplification image as shown in the inset of Figure 1B, some obvious wrinkles (see the arrows in the inset) in accordance with the characteristics of GO were observed,[19] suggesting that the Cu(tpa) MOF had been coated well with GO. From the TEM images of Cu(tpa) (inset of Figure 1C) and the Cu(tpa)-GO composite (Figure 1C), the well-defined cuboid-shaped Cu(tpa) and its combination with GO could be further confirmed. The inset of Figure 1D showed the electronic photos of Cu(tpa) (1), GO

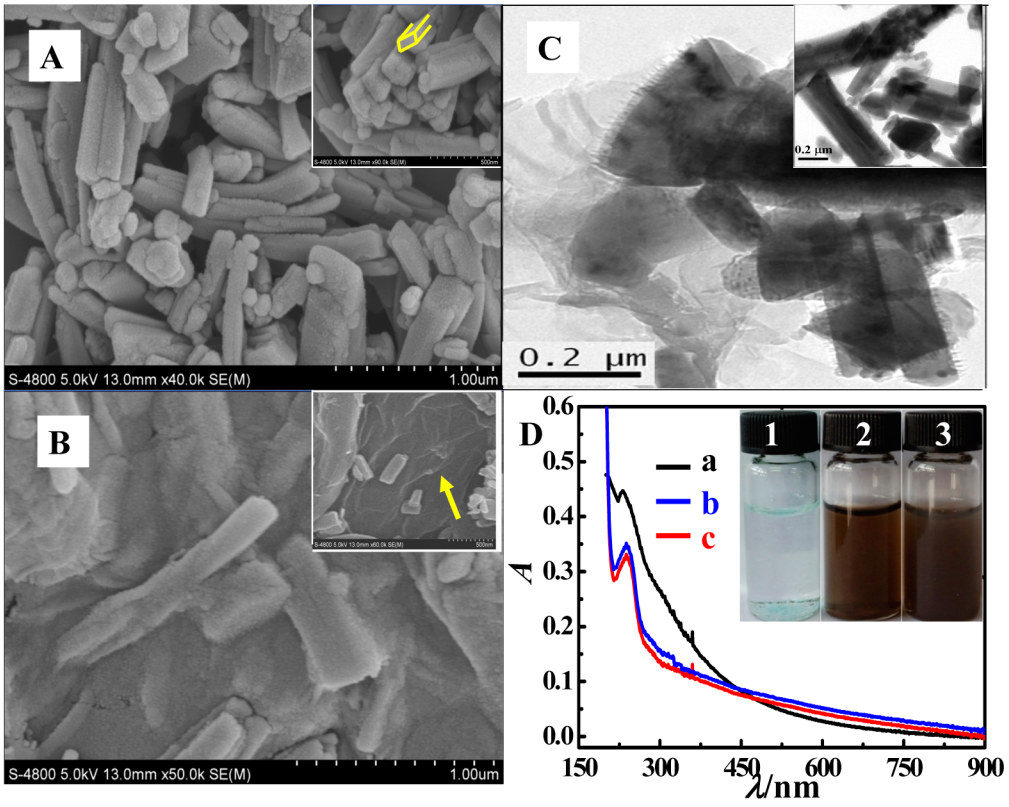

Figure 1. SEM images of Cu(tpa) (A) and Cu(tpa)-GO (B) with low resolution (main panel) and high resolution (inset). (C) TEM images of Cu(tpa)-GO (main panel) and Cu(tpa) (inset). (D) UV−vis absorption spectra of GO (a) and Cu(tpa)-GO before (b) and after (c) standing for 30 days. The inset in (D) shows the photographs of Cu(tpa) (1), GO (2), and Cu(tpa)-GO (3) aqueous dispersions.

(2), and Cu(tpa)-GO (3) aqueous dispersions. As seen, the GO aqueous solution showed a homogeneous black−brown color (Photo 2), indicating the as-prepared GO had good solubility in water, but for the aqueous solution of Cu(tpa), it was observed that a layer of light-blue powder appeared on the bottom of the vial within 20 min (Photo 1), which indicated that the synthesized Cu(tpa) MOF had very poor solubility and dispersibility in water. It was interesting that, when GO was mixed with Cu(tpa), a homogeneous brown dispersion without any precipitate was obtained (Photo 3), and this state could be maintained at least for one month, suggesting that the addition of GO could effectively improve the solubility and dispersibility of Cu(tpa).

In order to probe the binding mechanism of between Cu(tpa) and GO, the composite material was further characterized by UV−vis spectroscopy. As displayed in Figure 1D, the GO in water exhibited a broad absorption peak at 231 nm and a weak shoulder peak at about 300 nm (curve a), which could be assigned to $\pi \rightarrow \pi^*$ transitions of unoxidized aromatic C═C bonds and n $\rightarrow$ π^* transitions of C═O bonds, respectively.[20] While for the aqueous solution of Cu(tpa)-GO, it was found that the absorption peak of GO at 231 nm was red-shifted to 238 nm (curve b), indicating that the electronic conjugation within GO sheets had been restored after the reaction with Cu(tpa). This is likely due to the π electrons coupling between the terephthalate linker in the MOF framework and the unoxidized aromatic rings. Besides, the weak shoulder peak of GO at about 300 nm totally disappeared in the absorption curve of Cu(tpa)-GO. This indicated that GO might also interact with Cu(tpa) through the hydrogen bonding and/or the Cu−O coordination bond.[20] The UV−vis experiments also revealed that the absorption spectrum of Cu(tpa)-GO hardly changed after the solution was stored for a month (curve c), demonstrating that the Cu(tpa)-GO had excellent chemical stability in water.

Further evidence of the interaction between GO and Cu(tpa) was investigated by FT-IR spectroscopy as shown in Figure 2A. For GO (curve a), the bands at 3386 and 1726 cm^{-1} were assigned to the characteristic vibrations of O−H and C═O bonds, respectively. The peaks at 1232 and 1042 cm^{-1} could be ascribed to the C−O stretching vibrations of C−OH and C−O−C (epoxy), respectively. The peak at 1620 cm^{-1} was related to the skeletal vibration of unoxidized graphitic domains.[21] After interaction with Cu(tpa), it was found that the C═O peak of GO shifted to 1688 cm^{-1}, and peaks at 1620 cm^{-1} (skeletal vibrations), 1232 cm^{-1} (C−OH), and 1042 cm^{-1} (C−O−C) disappeared (curve c). These changes confirmed that the interactions between the two species were $\pi-\pi$ packing and hydrogen bonding.[22] In addition, the characteristic peaks of Cu(tpa) (curve b) were all present in the spectrum of the composite (curve c), testifying that the structure of Cu(tpa) MOF had not been changed upon incorporation with GO. The XRD patterns of GO (curve a), Cu(tpa) (curve b), and Cu(tpa)-GO (curve c) were displayed in Figure 2B. Through a comparison, it was found that all the diffraction peaks of the crystalline Cu(tpa) remained in the composite of Cu(tpa)-GO, suggesting that the crystallinity of the Cu(tpa) component had not been disrupted by the interaction with GO under sonication. The thermal stabilities of GO (curve a), Cu(tpa) (curve b), and Cu(tpa)-GO (curve c) were measured by thermogravimetric analysis (TGA) under a N_2 atmosphere. As seen in Figure 2C, the GO began to lose

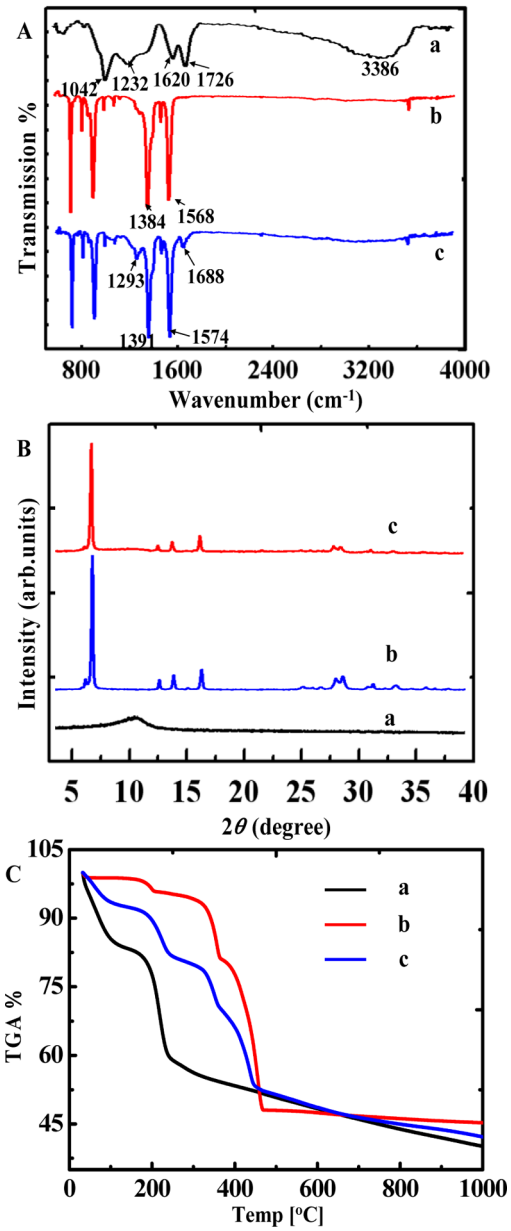

Figure 2. FT-IR spectra (A), XRD patterns (B), and TGA curves (C) of GO (a), Cu(tpa) (b), and Cu(tpa)-GO (c).

weight below 100 °C due to the thermal desorption of the water molecules physically adsorbed onto the hydrophilic GO surface. Then, a significant loss took place at around 200 °C, presumably due to the loss of the oxygen-containing functional groups present in GO.[23] The TGA curve of Cu(tpa) revealed that decomposition began at 150 °C, and the second weight loss step occurred in the range from 200 to 360 °C. When the temperature was up to 360 °C, a sharp increase in the weight loss appeared, indicating the Cu(tpa) structure had collapsed due to the removal of structural terephthalic acid linkers from the framework.[24] When the temperature was above 470 °C, the TGA curve became stable, suggesting no significant weight loss happened. The TGA curve of Cu(tpa)-GO composite showed the expected thermal behavior. The occurrence of the first loss was below 100 °C for GO adsorbed water molecules, and then, there were second and third losses at 190 and 330 °C, respectively. All these changes were quite consistent with the combined thermal decomposition behaviors of GO and Cu(tpa).

3.2. Electrochemical Properties of Cu(tpa)-EGR. The electrochemical reduction is a straightforward, efficient, and environmentally friendly approach for the preparation of the reduced form of GO.[25] In this work, GO in the Cu(tpa)-GO film was also electrochemically reduced to EGR by continuous cyclic scanning of Cu(tpa)-GO/GCE in 0.1 M PBS in the potential range from −1.5 to +0.6 V as reported in the literature.[18] The results were displayed in the main panel of Figure 3A. It was found that a pair of progressively increasing

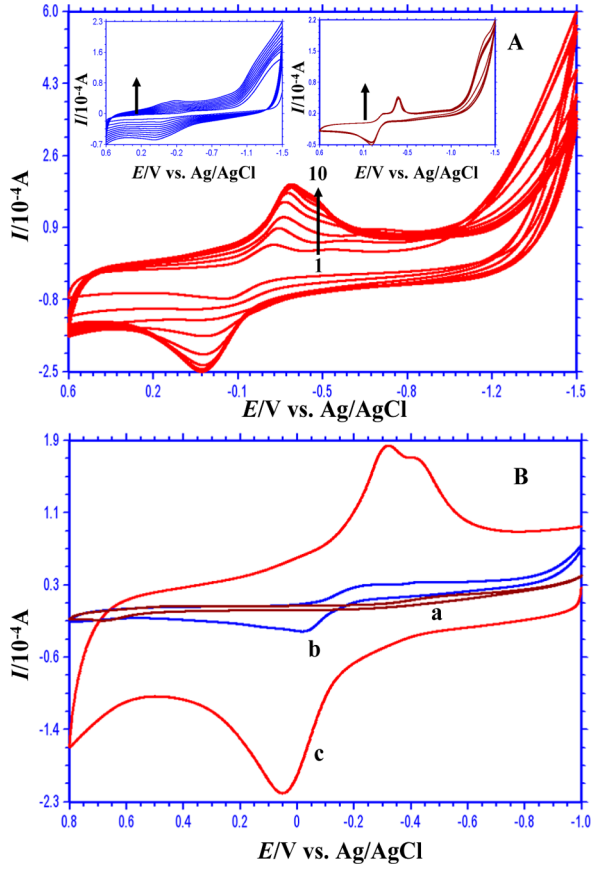

Figure 3. (A) Multiple sweep CVs of Cu(tpa)-GO/GCE (main panel), GO/GCE (left inset), and Cu(tpa)/GCE (right inset) in 0.1 M PBS (pH 7.0). (B) CVs of GO/GCE (a), Cu(tpa)-GO/GCE (b), and Cu(tpa)-EGR/GCE (c) in 0.1 M PBS (pH 7.0).

redox peaks was observed with the increase of the scan cycles, suggesting that the electrochemical response of the modified electrode gradually enhanced in the cyclic scan process. In addition to this, the background currents were also increased, suggesting that the capacitance currents that were related to the conductivity of the electrode interface also increased.[18] However, when the Cu(tpa) modified GCE (Cu(tpa)/GCE) was used as a control to test in the same way, it was found that almost no variation in the CV curves was observed throughout the scan process (right inset of Figure 3A). When the difference for these two electrodes was compared, it could be concluded that, with the increase of the sweep cycles, the GO nanosheets on Cu(tpa)-GO/GCE were continually transformed to the higher conductive EGR. Of course, it was noticeable that the peak-to-peak separation (ΔE_p) of the redox peaks on Cu(tpa)-GO/GCE also increased as the CV cycles increased, which

dx.doi.org/10.1021/am5019918 | ACS Appl. Mater. Interfaces 2014, 6, 11573−11580

conflicted with the above-mentioned conclusion; i.e., the conductivity of the modified film increased with the increase of the cycle number. This case might be caused by the following reason: At the initial stage, only the nonconductive GO existed in the composite film, so the electrochemical response at this stage only came from a small amount of Cu(tpa) that was in close contact with the GCE. As a result, the redox peak at this stage was small. Because this layer of Cu(tpa) molecules could directly communicate with electrons in the GCE, a small electron transfer resistance with a small ΔE_p was obtained. With the increase of the scan cycles, more and more GO in the composite film was transformed to the highly conductive EGR, which then acted as the electron pathway for the outer layer of Cu(tpa) and resulted in ever-increasing redox peaks on the electrode surface. However, when the outer Cu(tpa) molecules exchanged electrons with the GCE, they needed to overcome film-thickness caused resistance; therefore, a larger ΔE_p as compared with the initial stage was produced. When all the GO nanosheets in the composite film had been reduced, the CV curves became stable.

The continuous scanning of GO/GCE was also performed in PBS, and the results (left inset in Figure 3A) showed that the redox signal of GO/GCE ascribing to the electron transfer of oxygen-containing groups on GO was obviously smaller than that on Cu(tpa)-GO/GCE.[18] This indicated that the Cu(tpa) MOF in the composite could also significantly influence the electrochemistry of the modified electrode. To further probe this influence, the electrochemical behaviors of GO/GCE, Cu(tpa)/GCE, and Cu(tpa)-GO/GCE before and after electroreduction were investigated by CV in 0.1 M PBS (pH 7.0) with the potential range from −1.0 to 0.8 V. The results were shown in Figure 3B. As is well seen, no redox peaks were observed for the GO/GCE (curve a), suggesting that the GO layer was electrochemically inactive over this potential range. However, a clear oxidation peak at −0.017 V and two adjacent reduction peaks at −0.024 and −0.441 V appeared at Cu(tpa)-GO/GCE (curve b), which were very similar to the electrochemical response of Cu(tpa)/GCE during a continuous scan as presented in the right inset of Figure 3A. Thus, the redox peaks on Cu(tpa)-GO/GCE could be ascribed to the electroactive Cu(tpa). According to the literature,[26] the oxidation peak was assigned to electron transfer of $Cu^0 \rightarrow Cu^{2+}$, and the two reduction peaks to $Cu^{2+} \rightarrow Cu^+$ and $Cu^+ \rightarrow Cu^0$, respectively. After the Cu(tpa)-GO film was reduced to Cu(tpa)-EGR, it was found that redox peaks corresponding to the electrochemistry of Cu(tpa) were dramatically enhanced (curve c) due to the superior electrocatalytic effect of the EGR.[27]

3.3. Electrocatalysis of ACOP and DA by Cu(tpa)-EGR/GCE. To exploit the potential application of the Cu(tpa)-EGR composite, the electrochemical behaviors of two important drugs of ACOP and DA were investigated on the Cu(tpa)-EGR/GCE. Figure 4 shows the typical CVs of 0.1 mM ACOP and 0.1 mM DA on various electrodes in the potential range from 0 to +0.8 V. It was observed that two pairs of small and asymmetric redox peaks corresponding to the electron transfers of ACOP (at the higher potential range) and DA (at the lower potential range)[28,29] were detected at Cu(tpa)-GO/GCE (curve a). However, when the electro-reduced electrode (Cu(tpa)-EGR/GCE) was applied for determination, the redox peaks of ACOP and DA increased dramatically (curve d), and the redox process became more reversible as judged from the more symmetric peak profiles. In addition, the

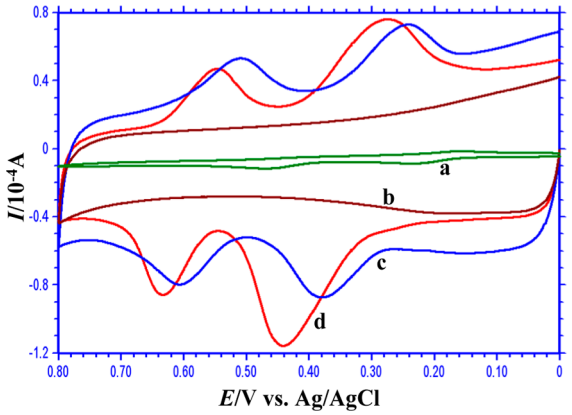

Figure 4. CVs of the 0.1 mM ACOP and 0.1 mM DA mixture at Cu(tpa)-GO/GCE (a), EGR/GCE (c), and Cu(tpa)-EGR/GCE (d) in 0.1 M PBS (pH 5.0). Curve b is the CV of Cu(tpa)-EGR/GCE in 0.1 M PBS (pH 5.0) without ACOP and DA.

electrochemical behavior of Cu(tpa)-EGR/GCE in PBS without ACOP and DA was tested, and the result showed that not any redox peak was observed under the same potential range (curve b). Therefore, it could be concluded that the composite material of Cu(tpa)-EGR had significant electrocatalysis toward ACOP and DA. As a control, the electrochemistry of ACOP and DA at EGR/GCE was also studied, and the result was depicted as curve c in Figure 4. Clearly, also two pairs of well-defined redox peaks were observed, but the intensities of all the peaks were obviously smaller than those at Cu(tpa)-EGR/GCE. This meant that the component of Cu(tpa) material in the composite film also had a positive effect on improving the electrochemical response of ACOP and DA, which was likely caused by the outstanding porous structure and favorable electron transfer mediating function of the electroactive Cu(tpa) MOF.

3.4. Electrochemical Parameters of ACOP and DA at Cu(tpa)-EGR/GCE. Figure 5A shows the dependence of CVs of ACOP and DA on the scan rate (ν). It was observed that all the peak currents (I_p) presented good linear correlations with ν at Cu(tpa)-EGR/GCE over the range from 20 to 400 mV s^{-1} (Figure 5B), suggesting adsorption-controlled processes of ACOP and DA at Cu(tpa)-EGR/GCE.[30,31] Additionally, the electrochemical parameters of electron transfer coefficient (α) and standard electron transfer rate constant (k_s) of ACOP and DA at the modified electrode were calculated according to the following Laviron's eqs 1−3.[32]

$$E_{pa} = E^{0'} + \frac{2.3RT}{(1-\alpha)nF}\log \nu \quad (1)$$

$$E_{pc} = E^{0'} - \frac{2.3RT}{\alpha nF}\log \nu \quad (2)$$

$$\log k_s = \alpha\log(1-\alpha) + (1-\alpha)\log \alpha - \log\frac{RT}{nFv} - \frac{(1-\alpha)\alpha nF\Delta E_p}{2.3RT} \quad (3)$$

where n is electron-transferred number of the electroactive species, E_{pa} and E_{pc} represent the oxidation and reduction peak potentials, respectively, and R, T, and F are in their usual significance. Through analyzing the data from Figure 5, it was obtained that the E_{pa} and E_{pc} had linear relationships with the

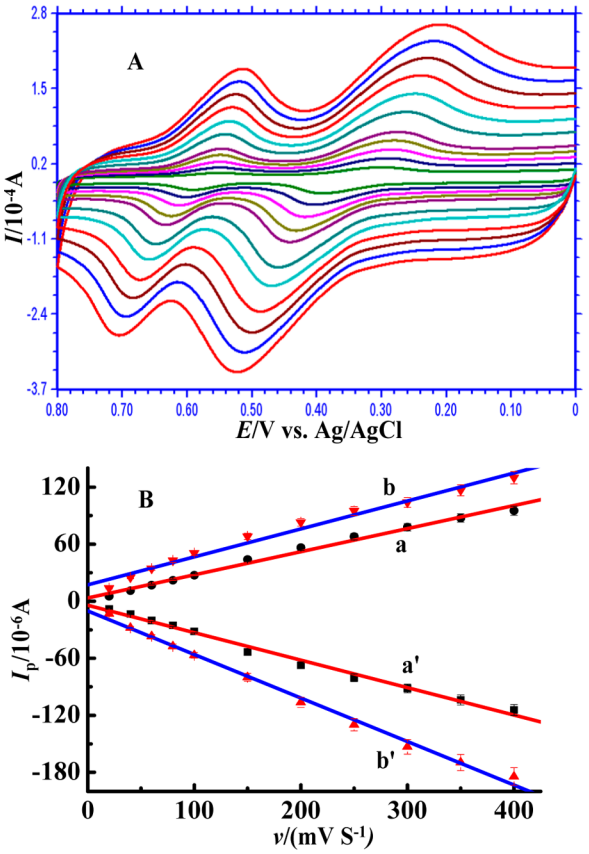

Figure 5. (A) CVs of a 0.1 mM ACOP and 0.1 mM DA mixture at Cu(tpa)-EGR/GCE with different scan rates (from inner to outer are 20, 40, 60, 80, 100, 150, 200, 250, 300, 350, and 400 mV s^{-1}, respectively.). (B) Plots of the peak currents (I_p) of ACOP (a and a′) and DA (b and b′) versus scan rates (v).

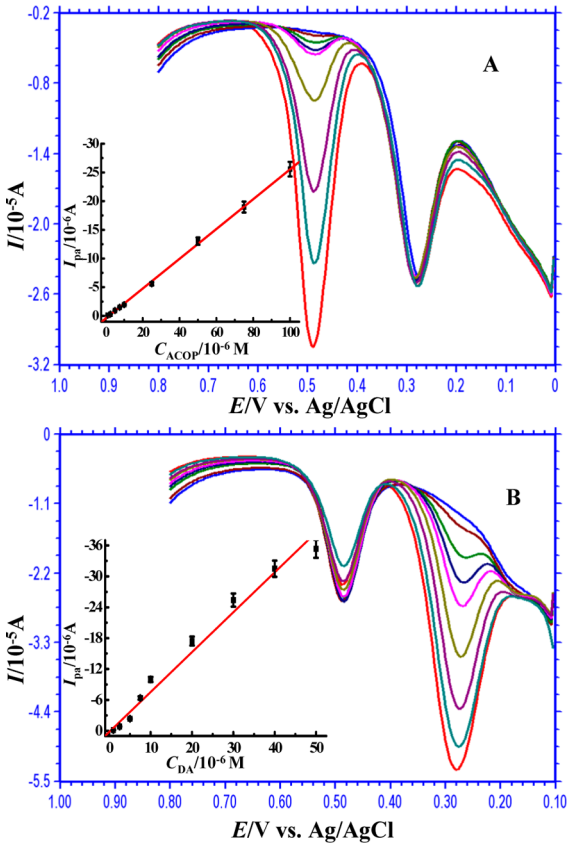

Figure 6. (A) DPVs of ACOP over a concentration range of 1.0 to 100 μM at Cu(tpa)-EGR/GCE in the presence of 20 μM DA in 0.1 M PBS (pH 5.0). (B) DPVs of DA over a concentration range of 1.0 to 50 μM at Cu(tpa)-EGR/GCE in the presence of 50 μM ACOP in 0.1 M PBS (pH 5.0). Insets in (A) and (B) are, respectively, the linear calibration plots of peak currents (I_{pa}) versus the concentrations of ACOP (C_{ACOP}) and DA (C_{DA}).

logarithm values of v (log v) for both ACOP and DA. The regression equations for ACOP were E_{pa}/V = 0.7336 + 0.1151 log v (V s^{-1}, γ = 0.9784) and E_{pc}/V = 0.5110 − 0.03497 log v (V s^{-1}, γ = 0.8993), and the regression equations for DA were E_{pa}/V = 0.5521 + 0.07393 log v (V s^{-1}, γ = 0.9817) and E_{pc}/V = 0.2029 − 0.05354 log v (V s^{-1}, γ = 0.9761). Then, on the basis of eqs 1 and 2, the values of α and n of ACOP were determined to be 0.77 and 2.2 and those of DA were 0.58 and 1.9, respectively. These indicated that both DA and ACOP underwent a two electrons transfer process at the modified electrode of Cu(tpa)-EGR/GCE, which was consistent with the results in the literature.[30,33] Furthermore, the values of the k_s of ACOP and DA were calculated to be 1.19 and 0.49 s^{-1} on the basis of eq 3.

3.5. Selective Determination of ACOP and DA. DPV is a powerful electrochemical technique that is often used for quantitative analysis because of its higher sensitivity and better resolution than CV.[34] Therefore, in this work, DPV was further utilized to investigate the analytical performance of the sensor to ACOP and DA. Figure 6A shows the DPVs of 20 μM DA in the presence of increasing amounts of ACOP. As is well seen, two well-defined and resolved peaks were observed, suggesting that the Cu(tpa)-EGR/GCE was very appropriate for the simultaneous determination of the two species as an electrochemical sensor. In addition, it was clear to see that the peaks at the lower potential corresponding to the electro-oxidation of DA remained constant throughout the tests. This meant that DA and its oxidative products did not irreversibly adsorb on the Cu(tpa)-EGR/GCE surface to interfere with the determination.[35] However, the peaks at the higher potential ascribing to the oxidation of ACOP were enhanced gradually with the increase of the ACOP concentrations, and the peak currents (I_{pa}) presented a good linear relationship with the ACOP concentration (C_{ACOP}) in the range from 1.0 to 100 μM with the linear equation of I_{pa}/μA = −0.2596 C_{ACOP} (μM) + 0.4352 (γ = 0.9996). With a signal-to-noise (S/N) = 3, the detection limits of ACOP were estimated to be 0.36 μM.

Similarly, when the solution of 50 μM ACOP with increasing amounts of DA was detected at Cu(tpa)-EGR/GCE by DPV, also two well-defined oxidation peaks were observed (Figure 6B). The DPV peak of ACOP remained constant, but the peaks of DA increased with the increase of DA concentrations (C_{DA}). The peak currents (I_{pa}) showed a good linear relationship with DA concentration (C_{DA}) in the range of 1.0 to 50 μM, with the linear equation of I_{pa}/μA = −0.7742 C_{DA} (μM) + 0.892 (γ = 0.9932). Also when S/N = 3, the detection limit of DA was estimated to be 0.21 μM. The above two assays also demonstrated that the ACOP (or DA) could be selectively determined by Cu(tpa)-EGR/GCE without affording the interference from each other. Table 1 summarized the comparison of analytical results of the other work with ours. Through the comparison, it could be determined that the sensor of Cu(tpa)-EGR/GCE presented in this work had comparable or better performance than the others, which opens

Table 1. Comparisons of Analytical Performance of ACOP and DA on Electrode Modified with Different Materials[a]

modified materials	test methods	linear ranges (μM)		detection limits (μM)		reference
		ACOP	DA	ACOP	DA	
GO	DPV		1−15		0.27	33
TiO_2-GR	DPV		5−200		2	36
MWCNTs	DPV	5−100		2.4		37
PMR/TiO_2-GR	DPV	0.25−50		0.025		38
PyC	DPV	15−225	18−270	1.4	2.3	39
f-MWCNTs	DPV	3−300	3−200	0.6	0.8	40
Cu(tpa)-EGR	DPV	1−100	1−50	0.36	0.21	this work

[a]Note: MWCNTs = multiwall carbon nanotubes; PMR/TiO_2-GR = TiO_2-graphene/poly(methyl red); PyC = thin pyrolytic carbon films; f-MWCNTs = acid functionalized multiwall carbon nanotubes.

Table 2. Determination of ACOP and DA in Human Serum and Urine Samples

	analyte	detected (μM)	added (μM)	found (μM)	recovery (%)	RSD (%)
serum 1	ACOP		20	20.3 ± 1.3	101	2.54
	DA		20	19.6 ± 1.6	98	1.80
urine 1	ACOP	1.5 ± 0.5	20	21.2 ± 1.2	99	2.52
	DA	1.2 ± 0.6	20	20.8 ± 1.6	98	1.82
urine 2	ACOP	1.8 ± 0.5	20	21.3 ± 1.2	98	2.53
	DA	1.0 ± 0.6	20	20.6 ± 1.6	98	1.81

a new way for the simultaneous and high-performance determination of ACOP and DA.

Furthermore, in order to evaluate the fabrication repeatability of the sensor, the prepared Cu(tpa)-EGR/GCE was used to repeatedly determine the response of a 25 μM ACOP and DA solution. The relative standard deviation (RSD) for seven measurements was 7.9%, suggesting the acceptable repeatability and precision, and the response of the modified electrode to a 25 μM ACOP and DA solution only decreased 5.47% of its initial response signal after being stored at 4 °C for 2 weeks, indicating good stability of the sensor.

3.6. Interference Studies. The potential interference for the determination of ACOP and DA was also studied. Under the optimal conditions, the electrochemical response of a 25 μM ACOP and DA solution was individually measured in the presence of different concentrations of the interferents. It was found that the common inorganic ions such as K^+, Na^+, NH_4^+, Ca^{2+}, Cl^-, SO_4^{2-}, and PO_4^{3-} in 100-fold excess had no influence on the peak currents of ACOP and DA since their peak current changes were below 5%. The common biological interferents such as hydroquinone, glucose, tyrosine, ascorbic acid, and L-cysteine also had no great interference to the response of ACOP and DA (signal change below 8%), suggesting that the sensor had excellent selectivity for determination of ACOP and DA.

3.7. Real Sample Determination. Real samples were analyzed by the standard addition method. In order to avoid the interferences of the complicated matrix in the real samples and fit into the linear ranges of ACOP and DA, only diluted urine and serum samples were added into the electrochemical cell. To ascertain the correctness of the results, the diluted samples mentioned above were spiked with certain amounts of ACOP and DA and then measured under the optimal conditions. The recovery of the spiked samples ranged between 98% and 101% (Table 2), indicating that the Cu(tpa)-EGR/GCE was reliable and sensitive enough for the determination of ACOP and DA in real samples.

4. CONCLUSION

In summary, we have demonstrated a facile method for preparation of a novel Cu(tpa) MOF-based composite using GO as the supporting carrier. Due to the high hydrophilicity of GO and its interaction with Cu(tpa), the composite shows excellent dispersibility and stability in water. After modification on GCE, the GO in the hybrid material was transformed to the reduced form (EGR) through a simple and effective electrochemical method, which made the modified film have a higher electrocatalytic property. When the modified electrode was utilized as a sensor model for the determination of DA and ACOP, it was found that high sensitivity and low interference of the two drugs were achieved. The fabricated sensor also showed great potential applications in the detection of ACOP and DA in serum and urine samples. Our present study opens a new avenue for extending the electrochemical application of the MOF-based composite materials.

AUTHOR INFORMATION

Corresponding Author

*E-mail: axiang236@126.com. Tel: +86-596-2591445. Fax: +86-596-2520035.

Notes

The authors declare no competing financial interest.

ACKNOWLEDGMENTS

The work is supported by the National Natural Science Foundation of China (No. 21275127), Program for New Century Excellent Talents in Fujian Province University (No. JA12204), Research Foundation of Fujian Education Department (JA12216), and Natural Science Foundation of Zhangzhou (ZZ2012J01).

REFERENCES

(1) Murray, L. J.; Dinca, M.; Long, J. R. Hydrogen Storage in Metal Organic Frameworks. *Chem. Soc. Rev.* **2009**, *38*, 1294−1314.

(2) Lee, J.; Farha, O. K.; Roberts, J.; Scheidt, K. A.; Nguyen, S. T.; Hupp, J. T. Metal Organic Framework Materials as Catalysts. *Chem. Soc. Rev.* **2009**, *38*, 1450−1459.

(3) Liu, B.; Shioyama, H.; Jiang, H.; Zhang, X.; Xu, Q. Metal−Organic Framework (MOF) as a Template for Syntheses of Nanoporous Carbons as Electrode Materials for Supercapacitor. *Carbon* **2010**, *48*, 456−463.
(4) Kitagawa, H. Metal−Organic Frameworks: Transported into Fuel Cells. *Nat. Chem.* **2009**, *1*, 689−690.
(5) James, S. L. Metal Organic Frameworks. *Chem. Soc. Rev.* **2003**, *32*, 276−288.
(6) Rowsell, J. L.; Yaghi, O. M. Metal−Organic Frameworks: A New Class of Porous Materials. *Microporous Mesoporous Mater.* **2004**, *73*, 3−14.
(7) Monzon, L. M.; Burke, F.; Coey, J. Optical, Magnetic, Electrochemical and Electrical Properties of 8-Hydroxyquinoline-Based Complexes with Al^{3+}, Cr^{3+}, Mn^{2+}, Co^{2+}, Ni^{2+}, Cu^{2+}, and Zn^{2+}. *J. Phys. Chem. C* **2011**, *115*, 9182−9192.
(8) Mao, J.; Yang, L.; Yu, P.; Wei, X.; Mao, L. Electrocatalytic Four Electron Reduction of Oxygen with Copper (II) Based Metal−Organic Frameworks. *Electrochem. Commun.* **2012**, *19*, 29−31.
(9) Li, Y.; Huangfu, C.; Du, H.; Liu, W.; Li, Y.; Ye, J. Electrochemical Behavior of Metal−Organic Framework MIL−101 Modified Carbon Paste Electrode: An Excellent Candidate for Electroanalysis. *J. Electroanal. Chem.* **2013**, *709*, 65−69.
(10) Zhang, Y.; Bo, X.; Luhana, C.; Wang, H.; Li, M.; Guo, L. Facile Synthesis of a Cu-Based MOF Confined in Macroporous Carbon Hybrid Material with Enhanced Electrocatalytic Ability. *Chem. Commun.* **2013**, *49*, 6885−6887.
(11) Hosseini, H.; Ahmar, H.; Dehghani, A.; Bagheri, A.; Tadjarodi, A.; Fakhari, A. R. A Novel Electrochemical Sensor Based on Metal−Organic Framework for Electro-Catalytic Oxidation of L-Cysteine. *Biosens. Bioelectron.* **2013**, *42*, 426−429.
(12) Dreyer, D. R.; Park, S.; Bielawski, C. W.; Ruoff, R. S. The Chemistry of Graphene Oxide. *Chem. Soc. Rev.* **2010**, *39*, 228−240.
(13) Byon, H. R.; Lee, S. W.; Chen, S.; Hammond, P. T.; Shao, H. Y. Thin Films of Carbon Nanotubes and Chemically Reduced Graphenes for Electrochemical Micro-Capacitors. *Carbon* **2011**, *49*, 457−467.
(14) Haque, A. M. J.; Park, H.; Sung, D.; Jon, S.; Choi, S. Y.; Kim, K. An Electrochemically Reduced Graphene Oxide Based Electrochemical Immunosensing Platform for Ultrasensitive Antigen Detection. *Anal. Chem.* **2012**, *84*, 1871−1878.
(15) William, S.; Hummers, J.; Richard, E. Preparation of Graphitic Oxide. *J. Am. Chem. Soc.* **1958**, *80*, 1339.
(16) Levasseur, B.; Petit, C.; Bandosz, T. J. Reactive Adsorption of NO_2 on Copper-Based Metal−Organic Framework and Graphite Oxide/Metal−Organic Framework Composites. *ACS Appl. Mater. Interfaces* **2010**, *2*, 3606−3613.
(17) Carson, C. G.; Hardcastle, K.; Schwartz, J.; Liu, X.; Hoffmann, C.; Gerhardt, R. A.; Tannenbaum, R. Synthesis and Structure Characterization of Copper Terephthalate Metal−Organic Frameworks. *Eur. J. Inorg. Chem.* **2009**, *2009*, 2338−2343.
(18) Liu, C.; Wang, K.; Luo, S.; Tang, Y.; Chen, L. Direct Electrodeposition of Graphene Enabling the One-Step Synthesis of Graphene−Metal Nanocomposite Films. *Small* **2011**, *7*, 1203−1206.
(19) Stankovich, S.; Dikin, D. A.; Piner, R. D.; Kohlhaas, K. A.; Kleinhammes, A.; Jia, Y.; Wu, Y.; Nguyen, S. T.; Ruoff, R. S. Synthesis of Graphene-Based Nanosheets via Chemical Reduction of Exfoliated Graphite Oxide. *Carbon* **2007**, *45*, 1558−1565.
(20) Li, D.; Muller, M. B.; Gilje, S.; Kaner, R. B.; Wallace, G. G. Processable Aqueous Dispersions of Graphene Nanosheets. *Nat. Nanotechnol.* **2008**, *3*, 101−105.
(21) Xu, Y.; Bai, H.; Lu, G.; Li, C.; Shi, G. Flexible Graphene Films via the Filtration of Water Soluble Noncovalent Functionalized Graphene Sheets. *J. Am. Chem. Soc.* **2008**, *130*, 5856−5857.
(22) Wang, H.; Hao, Q.; Yang, X.; Lu, L.; Wang, X. Graphene Oxide Doped Polyaniline for Supercapacitors. *Electrochem. Commun.* **2009**, *11*, 1158−1161.
(23) Pham, T. A.; Choi, B. C.; Lim, K. T.; Jeong, Y. T. A Simple Approach for Immobilization of Gold Nanoparticles on Graphene Oxide Sheets by Covalent bonding. *Appl. Surf. Sci.* **2011**, *257*, 3350−3357.
(24) Anbia, M.; Hoseini, V. Development of MWCNT@MIL-101 Hybrid Composite with Enhanced Adsorption Capacity for Carbon Dioxide. *Chem. Eng. J.* **2012**, *191*, 326−330.
(25) Xu, X.; Huang, D.; Cao, K.; Wang, M.; Zakeeruddin, S. M.; Grätzel, M. Electrochemically Reduced Graphene Oxide Multilayer Films as Efficient Counter Electrode for Dyesensitized Solar Cells. *Sci. Rep.* **2013**, *3*, 1−7.
(26) Shaikh, A. A.; Badrunnessa, M.; Firdaws, J.; Rahman, M. S.; Pasha, N. A.; Bakshi, P. K. A Cyclic Voltammetric Study of the Influence of Supporting Electrolytes on the Redox Behaviour of Cu(II) in Aqueous Medium. *J. Bangladesh Chem. Soc.* **2012**, *24*, 158−164.
(27) Wang, S. F.; Xie, F.; Hu, R. F. Carbon Coated Nickel Magnetic Nanoparticles Modified Electrodes as a Sensor for Determination of Acetaminophen. *Sens. Actuators, B* **2007**, *123*, 495−500.
(28) Guo, S.; Wen, S.; Zhai, Y. Z.; Dong, S. D.; Wang, E. Platinum Nanoparticle Ensemble on Graphene Hybrid Nanosheet One-pot, Rapid Synthesis, and Used as New Electrode Material for Electrochemical Sensing. *ACS Nano* **2010**, *4*, 3959−3968.
(29) Sun, C. L.; Lee, H. H.; Yang, J. M.; Wu, C. C. The Simultaneous Electrochemical Detection of Ascorbic Acid, Dopamine, and Uric Acid Using Graphene/Size-Selected Pt Nanocomposites. *Biosens. Bioelectron.* **2011**, *26*, 3450−3055.
(30) Zheng, M.; Gao, F.; Wang, Q.; Cai, X.; Jiang, S.; Huang, L.; Gao, F. Electrocatalytical Oxidation and Sensitive Determination of Acetaminophen on Glassy Carbon Electrode Modified with Graphene-Chitosan Composite. *Mater. Sci. Eng., C* **2013**, *33*, 1514−1520.
(31) Zhang, P.; Wu, F. H.; Zhao, G. C.; Wei, X. W. Selective Response of Dopamine in the Presence of Ascorbic Acid at Multi-Walled Carbon Nanotube Modified Gold Electrode. *Bioelectrochemistry* **2005**, *67*, 109−114.
(32) Laviron, E. General Expression of the Linear Potential Sweep Voltammogram in the Case of Diffusionless Electrochemical Systems. *J. Electroanal. Chem. Interfacial Electrochem.* **1979**, *101*, 19−28.
(33) Gao, F.; Cai, X.; Wang, X.; Gao, C.; Liu, S.; Gao, F.; Wang, Q. Highly Sensitive and Selective Detection of Dopamine in the Presence of Ascorbic Acid at Graphene Oxide Modified Electrode. *Sens. Actuators, B* **2013**, *186*, 380−387.
(34) Zhang, Y.; Wang, Y.; Wang, H.; Jiang, J. H.; Shen, G. L.; Yu, R. Q.; Li, J. Electrochemical DNA Biosensor Based on the Proximity Dependent Surface Hybridization Assay. *Anal. Chem.* **2009**, *81*, 1982−1987.
(35) Canevari, T. C.; Raymundo, P. A.; Landers, R.; Benvenutti, E. V.; Machado, S. A. Sol−Gel Thin Film Based Mesoporous Silica and Carbon Nanotubes for the Determination of Dopamine, Uric Acid and Paracetamol in Urine. *Talanta* **2013**, *116*, 726−735.
(36) Fan, Y.; Lu, H. T.; Liu, J. H.; Yang, C. P.; Jing, Q. S.; Zhang, Y. X.; Yang, X. K.; Huang, K. J. Hydrothermal Preparation and Electrochemical Sensing Properties of TiO_2−Graphene Nanocomposite. *Colloids Surf., B* **2011**, *83*, 78−82.
(37) Wan, Q.; Wang, X.; Yu, F.; Wang, X.; Yang, N. Effects of Capacitance and Resistance of MWNT Film Coated Electrodes on Voltammetric Detection of Acetaminophen. *J. Appl. Electrochem.* **2009**, *39*, 1145−1151.
(38) Xu, C. X.; Huang, K. J.; Fan, Y.; Wu, Z. W.; Li, J. Electrochemical Determination of Acetaminophen Based on TiO_2−Graphene/Poly(methyl red) Composite Film Modified Electrode. *J. Mol. Liq.* **2012**, *165*, 32−37.
(39) Keeley, G. P.; McEvoy, N.; Nolan, H.; Kumar, S.; Rezvani, E.; Holzinger, M.; Cosnier, S.; Duesberg, G. S. Simultaneous Electrochemical Determination of Dopamine and Paracetamol Based on Thin Pyrolytic Carbon Films. *Anal. Methods* **2012**, *4*, 2048−2053.
(40) Alothman, Z. A.; Bukhari, N.; Wabaidur, S. M.; Haider, S. Simultaneous Electrochemical Determination of Dopamine and Acetaminophen Using Multiwall Carbon Nanotubes Modified Glassy Carbon Electrode. *Sens. Actuators, B* **2010**, *146*, 314−320.